Learning-based method for k-space trajectory design in MRI

Sharma, Shubham; Hari, K.V.S.; Leus, Geert

DOI
10.1109/EMBC48229.2022.9871692

Publication date
2022

Document Version
Final published version

Published in
Proceedings of the 2022 44th Annual International Conference of the IEEE Engineering in Medicine & Biology Society (EMBC)

2022 44th Annual International Conference of
the IEEE Engineering in Medicine & Biology Society (EMBC)
Scottish Event Campus, Glasgow, UK, July 11-15, 2022

2022 44th Annual International Conference of the IEEE Engineering in Medicine & Biology Society (EMBC) | 978-1-7281-2782-8/22/$31.00 ©2022 IEEE | DOI: 10.1109/EMBC48229.2022.9871692

Learning-based method for k-space trajectory design in MRI

Shubham Sharma[1], K.V.S. Hari[1] and Geert Leus[2]

***Abstract*— Variable density sampling of the k-space in MRI is an integral part of trajectory design. It has been observed that data-driven trajectory design methods provide a better image reconstruction as compared to trajectories obtained from a fixed or a parametric density function. In this paper, a data-driven strategy has been proposed to obtain non-Cartesian continuous k-space sampling trajectories for MRI under the compressed sensing framework (greedy non-Cartesian (GNC)). A stochastic version of the algorithm (stochastic greedy non-Cartesian (SGNC)) is also proposed that reduces the computation time. We compare the proposed trajectory with a traveling salesman problem (TSP)-based trajectory and an echo planar imaging-like trajectory obtained by a greedy method called stochastic greedy-Cartesian (SGC) algorithm. The training images are taken from knee images of the fastMRI dataset. It is observed that the proposed algorithms outperform the TSP-based and the SGC trajectories for similar read-out times.**

***Index Terms*— MRI, variable-density sampling, data-driven, k-space trajectory design.**

I. Introduction

Magnetic resonance imaging (MRI) is a powerful non-invasive tool for high quality soft tissue imaging. The physics of the MRI system results in a signal that can be directly mapped to the frequency domain, also known as the k-space in the MRI community. The k-space is traversed by varying the linear magnetic gradients ($k_i(t) = \int_0^t \gamma G_i(\tau)d\tau,\ i \in \{x, y, z\}$) which are limited by their magnitude ($G_{\max}$) and slew rate ($S_{\max}$) [1]. The most common k-space trajectory used in practice is the Cartesian trajectory. In this method, the k-space is traversed one horizontal line at a time in a single excitation. The k_x-axis is called the frequency encoding direction and the k_y-axis is called the phase encoding direction. Each horizontal line is called a phase encode.

MRI is inherently limited by its data acquisition time. Methods such as compressed sensing (CS) [2] and parallel imaging [3] have significantly brought down the acquisition time by utilizing redundancies in the image and the frequency domains. In this paper, we address the problem of k-space trajectory design in 2D under the CS framework [4], [5], [6], [7], [8]. In recent years, in contrast to the model-based random variable density (VD) sampling methods, data-driven methods have been observed to provide better sampling patterns that significantly improve the reconstruction performance. These methods aim to learn and adapt sampling patterns for specific anatomical structures and reconstruction methods [9], [10], [11]. The Bayesian approach in [9] optimizes Cartesian or any arbitrary trajectory, this approach is, however, computationally expensive. Another data-driven approach is explored in [10] where an integer programming problem is solved to minimize the Cramèr-Rao bound on the reconstruction. The method in [12] provides improvement in reconstruction using non-Cartesian trajectories with gradient constraints imposed. However, this approach does not consider a data-driven learning.

Many methods (model-based and data-driven) consider subsampling in the phase encoding direction for a Cartesian trajectory. However, non-Cartesian trajectories such as spiral, radial, rosette etc. offer advantages such as being more robust to motion-related artifacts and better utilization of the gradient capacity [13], [14], [15]. Hence, we propose a learning-based greedy algorithm to obtain a continuous VD non-Cartesian trajectory for a specific anatomical structure. The proposed algorithms differ from the greedy algorithms in [11] and [16] as our methods are based on region-wise distance-based rules to learn the next points along the trajectory and the resultant trajectories utilize VD sampling on both k_x and k_y axes on the k-space.

II. Learning-based VD Trajectory Design

The desired image $\mathbf{X}\in\mathbb{C}^{N\times N}$ is assumed to come from an unknown probability distribution P. The set of p fully sampled training images $\mathcal{X}=\{\mathbf{X}_1, \mathbf{X}_2, ..., \mathbf{X}_p\}$, $\mathbf{X}_i\in\mathbb{C}^{N\times N}$ are assumed to be well representative of the anatomical structure. A set of sample points Ω on the k-space when connected are referred to as a continuous trajectory. A continuous trajectory is desired as the trajectory is traversed using gradient coils and to sample individual points on the k-space is not optimal in terms of time and utilization of hardware constraints. The problem of finding an optimal set of points (Ω^*) forming a feasible trajectory in the k-space, i.e., satisfying the gradient constraints, in terms of imaging a given anatomy can be formulated as

$$\Omega^* = \arg\max_{\Omega\in\mathcal{S}} \mathbb{E}_{\mathbf{X}\sim P}\left[\eta_\Omega(\mathbf{X}, \hat{\mathbf{X}})\right] \tag{1}$$

where $\mathcal{S}$ is the set of feasible trajectories, $\hat{\mathbf{X}}$ is the reconstructed image and $\eta_\Omega(\mathbf{X}, \hat{\mathbf{X}})$ is a performance metric, for instance, peak signal-to-noise ratio (PSNR) or structural similarity index (SSIM). This is empirically solved using

$$\Omega^* = \arg\max_{\Omega\in\mathcal{S}} \frac{1}{p}\sum_{i=1}^{p} \eta_\Omega(\mathbf{X}_i, \hat{\mathbf{X}}_i) \tag{2}$$

with p training images. Note that in addition to the sample points Ω, the reconstruction method highly influences the quality of the reconstructed image [17]. Problem (2) is a combinatorial problem and an approximate solution can be found using greedy algorithms. For instance, in [11], $\mathcal{S}$ is taken as the set of all eligible phase encodes, i.e., horizontal lines along the k_x direction. We propose a greedy

[1]Shubham Sharma and K.V.S. Hari are with the Department of Electrical Communication Engineering, Indian Institute of Science, Bangalore, India shubham@iisc.ac.in, hari@iisc.ac.in

[2]Geert Leus is with the Department of Microelectronics, Delft University of Technology, The Netherlands G.J.T.Leus@tudelft.nl

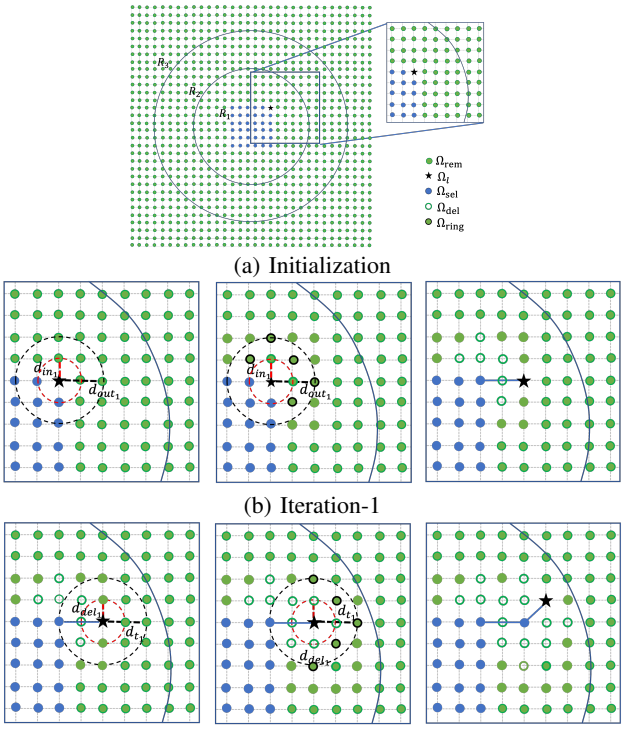

(a) Initialization

(b) Iteration-1

(c) Iteration-2

Fig. 1: Demo of greedy non-Cartesian (GNC) algorithm. A 32×32 k-space grid (Ω_{grid}) is divided into $r = 3$ regions. (a) Initialization step with 6×6 center points (Ω_c) in Ω_{sel}, the remaining points (Ω_{rem}) and the chosen Ω_l. (b) describes the first iteration. Ω_l is in R_1. Next, identify Ω_{ring} and update Ω_{rem}. Update Ω_l that results in the best mean reconstruction performance among all Ω_{ring}. (c) describes the second iteration.

approach inspired by the method in [11]. The proposed method provides region-wise distance-based rules to add sample points that provide the best average performance on the training images to construct continuous trajectories for 2D sampling of the k-space. Such region-wise distance-based rules facilitate a variable density sampling under the non-Cartesian sampling scheme. This is done by finding a continuous trajectory $\Omega \in \mathcal{C}$, where $\mathcal{C}$ is the set of continuous trajectories (not necessarily satisfying the gradient constraints). This infeasible trajectory is later made feasible using the method in [18]. The proposed greedy algorithm is discussed below.

A. Greedy Non-Cartesian (GNC) Algorithm

The algorithm aims to obtain a continuous path by adding one sample point at a time to the already selected set of points on the Cartesian grid. The sample point in the vicinity of the last sampled point (and not previously sampled) that results in the best mean reconstruction performance on the training images is included in the trajectory. The proposed algorithm utilizes the prior knowledge that the k-space center needs to be sampled more densely as compared to the boundary region. For this, we divide the 2D k-space sampled at the Cartesian grid (Ω_{grid}), extending from $-k_{\max}$ to $k_{\max}$ along the k_x and k_y axes, into r circular regions centered at the center of the k-space, denoted by the set $R = \{R_1, R_2, ...R_r\}$. Each of these regions describes a set of grid points with 2D frequencies denoted as $\Omega_j = [k_{x_j} \quad k_{y_j}]^T \in \Omega_{\text{grid}}$. The regions are used to define a set of rules to set a step size for the next optimal point to be selected. These rules help achieve a VD sampling such that a region that is closer to the center of the k-space is set to have a smaller step size to densely sample that region. Similarly, a region farther from the center will have a bigger step size to sparsely sample that region.

Algorithm 1 describes the proposed greedy method. The set of points selected from the Cartesian grid Ω_{grid} is denoted as Ω_{sel}. The center of the k-space with grid points Ω_c consisting of the center $n_c \times n_c$ points are sampled first. The last selected point Ω_l can be initialized as any outermost point of Ω_{sel}. Points in the ring given by two concentric circles (Ω_l as the center) with radius of the inner circle being d_{in} and the radius of the outer circle being d_{out} are considered. Each of the *nearby* points inside the ring, denoted by Ω_{ring}, are used to find the average reconstruction performance using the reconstruction method $\mathcal{R}(\Omega, \mathbf{X})$ when included with Ω_{sel}. The one point that gives the best reconstruction performance on the training images is included in the set Ω_{sel}. All the points inside the outer circle at distances less than d_{out} from Ω_l are removed from further consideration. This is repeated till no points remain in the grid.

Bigger steps are taken as we move away from the center, i.e., $d_{\text{in}_1} < d_{\text{in}_2} < ... < d_{\text{in}_r}$ and $d_{\text{out}_1} < d_{\text{out}_2} < ... < d_{\text{out}_r}$. It is assumed that inclusion of a grid point will not decrease the reconstruction performance. It is to be noted that even though the points are taken from a Cartesian grid, these trajectories are called non-Cartesian. This is done, firstly, to emphasize that these do not traverse the k-space in horizontal lines as is done in a Cartesian trajectory. Secondly, the final feasible trajectory will introduce new non-Cartesian sample points along the trajectory, making this a non-Cartesian trajectory.

Figure 1 illustrates the different sets on the k-space Cartesian grid for better visualization. This example consists of 3 regions. The initialization step with a 6×6 center region and two iterations that select two optimal points are shown.

B. Stochastic Greedy Non-Cartesian (SGNC) Algorithm

The large size of the training data and the search in 2D space make the GNC algorithm computationally very expensive. Similar to the stochastic version of the GC algorithm in [16], referred to as the stochastic GC (SGC) algorithm here, a stochastic version of the GNC algorithm is proposed. This is referred to as the stochastic greedy non-Cartesian (SGNC) algorithm.

The SGNC algorithm chooses a path (of a set of points) from multiple random paths instead of just one point starting from the last selected point Ω_l. In this method, first a subset $\Omega'_{\text{ring}} \subset \Omega_{\text{ring}}$ is randomly chosen with $|\Omega'_{\text{ring}}| = n_{\text{path}}$. Here, Ω_{ring} is chosen as described in the GNC algorithm. At each $\Omega \in \Omega'_{\text{ring}}$, a random path with n_p points is generated by randomly choosing one nearby point from the previously selected point in accordance with the distance

Algorithm 1: Greedy non-Cartesian (GNC) algo.

Input: $\mathcal{X}$, Ω_{grid}, Ω_c, R, d_{in}, d_{out}
Result: GNC Trajectory $\Omega_{\text{GNC}} = \Omega_{\text{sel}}$.
// Initialization (Refer Fig. 1(a))
$\Omega_{\text{sel}} \leftarrow \Omega_c$
$\Omega_l \leftarrow$ an outermost point in Ω_{sel}
$\Omega_{\text{rem}} \leftarrow \Omega_{\text{grid}} \setminus \Omega_{\text{sel}}$
// Repeat until no grid points remaining (Refer Fig. 1(b),(c))
while $\Omega_{\text{rem}} \neq \varnothing$ **do**
  ind $\leftarrow i$ if $\Omega_l \in R_i$ // Region of the last selected point
  $\Omega_{\text{ring}} \leftarrow \{\Omega_i \in \Omega_{\text{rem}} : d_{\text{in}_{\text{ind}}} \leq dist(\Omega_l, \Omega_i) \leq d_{\text{out}_{\text{ind}}}\}$
  // For all points inside the ring
  for $\Omega_i \in \Omega_{\text{ring}}$ **do**
    $\Omega_{\text{sel}'} = \Omega_{\text{sel}} \cup \Omega_i$
    $\hat{\mathbf{X}}_j \leftarrow \mathcal{R}(\Omega_{\text{sel}'}, \mathbf{X}_j), \forall \mathbf{X}_j \in \mathcal{X}$
    $\eta_{\Omega_i} \leftarrow \frac{1}{p} \sum_{j=1}^{p} \eta_{\Omega_{\text{sel}'}}(\mathbf{X}_j, \hat{\mathbf{X}}_j)$
  end
  $\Omega_l \leftarrow \arg\max_{\Omega_i} \eta_{\Omega_i}$
  $\Omega_{\text{sel}} \leftarrow \Omega_{\text{sel}} \cup \Omega_l$
  $\Omega_{\text{del}} \leftarrow \{\Omega_i \in \Omega_{\text{rem}} : dist(\Omega_l, \Omega_i) \leq d_{\text{out}_{\text{ind}}}\}$
  $\Omega_{\text{rem}} \leftarrow \Omega_{\text{rem}} \setminus \Omega_{\text{del}}$
end

rules described in the GNC algorithm. This reduces the computational load manifold. Also note that although the GNC and SGNC algorithms result in a set of points on the k-space, the sequence in which these points are selected results in piecewise continuous paths that form the GNC and SGNC trajectories, respectively.

The proposed algorithms can also be used for Cartesian sampling by dividing the k-space into rectangular regions above and below the $k_y = 0$ line instead of circular regions. A few center horizontal lines can be sampled during initialization and any one of the extreme phase encodes could be used as Ω_l. Similar region-wise distance-based rules can be used to remove some phase encodes from consideration and to add some other phase encodes for consideration.

III. Numerical Experiments

A. Simulation Setup

We consider the fastMRI knee database [19]. The single-coil training dataset comprises of 973 volumes with 34742 slices of knee images. We considered the center 12 slices of each volume to learn the trajectory. We compare the performance of the proposed greedy algorithms with a non-Cartesian trajectory based on the traveling salesman problem (TSP) [20] with points randomly sampled from the density function $\propto \frac{1}{|k|^2}$ and the SGC trajectory. Four-shot trajectories are used for a more practical implementation. For the TSP, GNC and SGNC trajectories the k-space is divided into four quadrants and each quadrant is traversed in one excitation. The phase encodes obtained from the SGC algorithm are used to obtain a 4-shot trajectory by connecting the selected phase encoding directions like that of an EPI trajectory [21]. This is referred to as EPI-like SGC trajectory. The trajectories considered are made feasible using the method in [18] with $G_{\max} = 40$ mT/m and $S_{\max}$ of 150 mT/m/s and hence the corresponding trajectories could be implemented in a scanner. The number of sample points in the feasible trajectories (denoted, m) are much higher than the original ones (denoted, n). The read-out time T is calculated as $T = m/f_s$, where $f_s = 250$ kHz is the sampling frequency. NESTA [22] is used to reconstruct images while learning the trajectory for all the greedy algorithms as it provides a really fast reconstruction when the points lie on the grid. PSNR is used as the metric η_Ω to compare the performance during learning. The k-space data is obtained from the 2D DFT of the complex training images. Also note that since the points on the feasible trajectories do not necessarily lie on the grid, we use the non-uniform fast Fourier transform (NUFFT) for the reconstruction of an image $\mathbf{X}$ using

$$\hat{\mathbf{X}} = \arg\min_{\mathbf{X}} \|\text{NUFFT}(\mathbf{X}) - \mathbf{Y}\|_2^2 + \lambda \|\mathbf{X}\|_{\text{TV}} \qquad (3)$$

where $\mathbf{Y}$ is the k-space data, λ is the weighting parameter and $\|\cdot\|_{\text{TV}}$ is the total variation norm.

For the GNC and SGNC algorithms, the k-space is divided into 6 regions given by $f = \{0, \frac{k_{\max}}{6}, \frac{k_{\max}}{4}, \frac{k_{\max}}{3}, \frac{k_{\max}}{2}, \frac{3k_{\max}}{4}\}$. d_{in_i} and d_{out_i} are taken as $\{0, 2, 5, 14, 35, 90\}$ and $\{2, 3, 4, 6, 9, 14\}$, respectively for $i \in \{1, ..., 6\}$. These are corresponding to $n_{\text{del}} = \{0, 1, 2, 4, 7, 12\}$. These distances result in a trajectory that takes $\sim$40 ms read-out time per shot. A feasible TSP trajectory with similar read-out time per shot is obtained with 3200 points sampled from the density function $\propto \frac{1}{|k|^2}$. For the EPI-like SGC trajectory, 50% phase encodes provide a similar read-out time.

B. Results and Discussion

Multiple trajectories were learned using the SGNC algorithm with the distance rules as discussed previously by varying the number of random paths (n_{path}), the number of images for training (n_{tr}) and the number of points on each path (n_{p}). Their reconstruction performance was compared for five randomly chosen test images. It was observed that there was no significant difference in the performance by having a higher n_{path} or by using a large n_{tr}. The used and recommended values for the SGNC algorithm are $n_{\text{path}} = 3$, $n_{\text{tr}} = 1$ and $n_{\text{p}} = 5$. The chosen trajectories are shown at the top row in Fig. 2.

TABLE I: Mean performance on 500 randomly selected images and 100 best performing images in terms of PSNR (out of 500) from the test dataset of knee fastMRI database.

Trajectory	Read-out time	500 test images		Best 100 test images	
		SSIM	PSNR	SSIM	PSNR
EPI-like SGC	39.06 ms	**0.5608**	25.31 dB	0.6854	28.65 dB
TSP	40.45 ms	0.5436	27.51 dB	0.7372	32.09 dB
SGNC	40.88 ms	0.5550	**27.94** dB	**0.7505**	**32.76** dB

Table I gives the mean reconstruction performance of the EPI-like SGC, TSP-based and SGNC trajectories for 500 randomly chosen knee images from the fastMRI single-coil test database. Many of these images are noisy and hence the average reconstruction performance is quite poor. The table also shows the mean of the best 100 out of the 500 test images for each trajectory. It was observed that more than 90 out of the 100 best performing test images showed common results for the three trajectories considered here. It is observed that the non-Cartesian trajectories (TSP-based and SGNC) provide better reconstruction performance in terms of PSNR compared to the EPI-like SGC trajectories. The SGNC trajectory results in a mean PSNR of 27.94 dB.

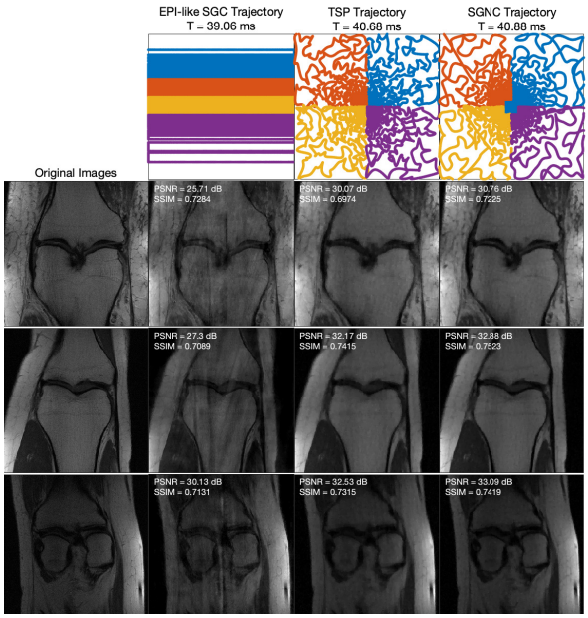

Fig. 2: The top row shows the four-shot feasible SGC, TSP and SGNC trajectories (each shot represented with a different colour). Original and reconstructed images using the three trajectories are shown.

This is significantly better than the mean PSNR of 25.31 dB for the EPI-like trajectory. The performance of the SGNC trajectory is comparable to the TSP-based trajectories which result in a mean PSNR of 27.51 dB.

Three test images (from the best 100 test images that were common for all methods) reconstructed using the EPI-like SGC, TSP and SGNC trajectories are shown in Fig. 2. Although the improvement with SGNC trajectories isn't as significant in terms of SSIM and PSNR, it can be seen in the figure that the reconstructed images from the SGNC trajectories are noticeably better. Simulations were performed to test the robustness of the three trajectories for off-resonance effects and gradient imperfection. The SGNC trajectory is observed to be less sensitive to these system imperfections (not illustrated here).

The reconstruction method used in this work is CS reconstruction with total variation (TV) sparsity. More recently, deep learning-based reconstruction methods are gaining popularity and can also be utilized by using a pre-trained reconstruction network. The trajectory and the corresponding reconstruction performances would be different when different reconstruction methods are utilized.

IV. Conclusion

In this paper, the problem of designing non-Cartesian k-space trajectories is considered. A data-driven greedy approach (GNC algorithm) is used to learn the best k-space sample points on the 2D Cartesian grid for a set of training images. The trajectory is built point-by-point in the proposed method. A faster algorithm (SGNC algorithm) is used to build the trajectory multiple points at a time by constructing multiple random paths and choosing the one that provides the best reconstruction performance on average for the training image. This results in trajectories that provide an improvement in the test images as compared to the EPI-like trajectories learned using the SGC algorithm and the TSP-based trajectories from a fixed density function.

V. Acknowledgment

The authors would like to thank the Ministry of Electronics and Information Technology (MeitY), India for the financial support to conduct this work. We are also grateful to the IISc-TU Delft collaboration agreement.

References

[1] R. B. Buxton, *Introduction to functional magnetic resonance imaging: principles and techniques*. Cambridge University Press, 2009.

[2] M. Lustig, D. Donoho, and J. M. Pauly, "Sparse MRI: The application of compressed sensing for rapid MR imaging," *J. of MRM*, vol. 58, no. 6, pp. 1182–1195, 2007.

[3] K. P. Pruessmann, M. Weiger, M. B. Scheidegger, P. Boesiger *et al.*, "SENSE: sensitivity encoding for fast MRI," *J. of MRM*, vol. 42, no. 5, pp. 952–962, 1999.

[4] M. Lustig, J. H. Lee, D. L. Donoho, and J. M. Pauly, "Faster imaging with randomly perturbed, under-sampled spirals and l1 reconstruction," in *Proc. of ISMRM*, 2005, p. 685.

[5] A. Bilgin, T. Trouard, A. Gmitro, and M. Altbach, "Randomly perturbed radial trajectories for compressed sensing MRI," in *Proceedings of ISMRM*, vol. 16, 2008, p. 3152.

[6] R. Willett, "Errata: Sampling trajectories for sparse image recovery," 2011.

[7] H. Wang, X. Wang, Y. Zhou, Y. Chang, and Y. Wang, "Smoothed random-like trajectory for compressed sensing MRI," in *IEEE EMBC*. IEEE, 2012, pp. 404–407.

[8] N. Chauffert, P. Weiss, J. Kahn, and P. Ciuciu, "A projection algorithm for gradient waveforms design in magnetic resonance imaging," *IEEE Trans. on Medical Imaging*, vol. 35, no. 9, pp. 2026–2039, 2016.

[9] M. Seeger, H. Nickisch, R. Pohmann, and B. Schölkopf, "Optimization of k-space trajectories for compressed sensing by bayesian experimental design," *J. of MRM*, vol. 63, no. 1, pp. 116–126, 2010.

[10] J. P. Haldar and D. Kim, "OEDIPUS: An experiment design framework for sparsity-constrained MRI," *IEEE Trans. on Medical Imaging*, vol. 38, no. 7, pp. 1545–1558, 2019.

[11] B. Gözcü, R. K. Mahabadi, Y.-H. Li, E. Ilıcak, T. Cukur, J. Scarlett, and V. Cevher, "Learning-based compressive MRI," *IEEE Transactions on Medical Imaging*, vol. 37, no. 6, pp. 1394–1406, 2018.

[12] C. Lazarus, P. Weiss, N. Chauffert, F. Mauconduit, L. El Gueddari, C. Destrieux, I. Zemmoura, A. Vignaud, and P. Ciuciu, "SPARKLING: variable-density k-space filling curves for accelerated T2*-weighted MRI," *J. of MRM*, vol. 81, no. 6, pp. 3643–3661, 2019.

[13] D.-h. Kim, E. Adalsteinsson, and D. M. Spielman, "Simple analytic variable density spiral design," *J. of MRM*, vol. 50, no. 1, pp. 214–219, 2003.

[14] S. Sharma, K. Hari, and G. Leus, "Space filling curves for MRI sampling," in *IEEE ICASSP*. IEEE, 2020, pp. 1115–1119.

[15] S. Sharma, M. Coutino, S. P. Chepuri, G. Leus, and K. Hari, "Towards a general framework for fast and feasible k-space trajectories for MRI based on projection methods," *J. of MRI*, vol. 72, pp. 122–134, 2020.

[16] T. Sanchez and et al., "Scalable learning-based sampling optimization for compressive dynamic MRI," in *IEEE ICASSP*. IEEE, 2020, pp. 8584–8588.

[17] C. D. Bahadir, A. Q. Wang, A. V. Dalca, and M. R. Sabuncu, "Deep-learning-based optimization of the under-sampling pattern in MRI," *IEEE Trans. on Computational Imaging*, vol. 6, pp. 1139–1152, 2020.

[18] M. Lustig, S.-J. Kim, and J. M. Pauly, "A fast method for designing time-optimal gradient waveforms for arbitrary k-space trajectories," *IEEE Trans. on Medical Imaging*, vol. 27, no. 6, pp. 866–873, 2008.

[19] J. Z. et al., "fastMRI: An open dataset and benchmarks for accelerated MRI," 2018.

[20] N. Chauffert, P. Ciuciu, J. Kahn, and P. Weiss, "Travelling salesman-based variable density sampling," *SampTA*, pp. 509–512, 2013.

[21] P. Mansfield, "Multi-planar image formation using NMR spin echoes," *Journal of Physics: Solid State Physics*, vol. 10, no. 3, p. L55, 1977.

[22] S. Becker, J. Bobin, and E. J. Candès, "NESTA: A fast and accurate first-order method for sparse recovery," *SIAM J. on Imaging Sciences*, vol. 4, no. 1, pp. 1–39, 2011.